Journal of Zhejiang University-SCIENCE A (Applied Physics & Engineering) 2025 26(1):66-77
www.jzus.zju.edu.cn; www.springer.com/journal/11582
E-mail: jzus_a@zju.edu.cn

Research Articles

https://doi.org/10.1631/jzus.A2300594

Positioning error prediction and compensation for the multi-boom working mechanism of a drilling jumbo

Yuming CUI[1], Songyong LIU[2]✉, Zhengqiang SHU[2], Zhenli LV[2], Lie LI[1]

[1]*School of Mechatronic Engineering, Jiangsu Normal University, Xuzhou 221116, China*
[2]*School of Mechatronic Engineering, China University of Mining and Technology, Xuzhou 221116, China*

Abstract: A rock-drilling jumbo is the main piece of tunneling equipment used in the energy and infrastructure industries in various countries. The positioning accuracy of its drilling boom greatly affects tunneling efficiency and section-forming quality of mine roadways and engineering tunnels. In order to improve the drilling-positioning accuracy of a three-boom drilling jumbo, we established a kinematics model of the multi-degree-of-freedom (multi-DOF) multi-boom system, using the improved Denavit-Hartenberg (D-H) method, and obtained the mapping relationship between the end position and the amount of motion of each joint. The error of the inverse kinematics calculation for the drilling boom is estimated by an analytical method and a global search algorithm based on particle swarm optimization (PSO) for a straight blasting hole and an inclined blasting hole. On this basis, we propose a back-propagation (BP) neural network optimized by an improved sparrow search algorithm (ISSA) to predict the positioning error of the drilling booms of a three-boom drilling jumbo. In order to verify the accuracy of the proposed error compensation model, we built an automatic-control test platform for the boom, and carried out a positioning error compensation test on the boom. The results show that the average drilling-positioning error was reduced from 9.79 to 5.92 cm, and the error was reduced by 39.5%. Therefore, the proposed method effectively reduces the positioning error of the drilling boom, and improves the accuracy and efficiency of rock drilling.

Key words: Multi-boom rock-drilling jumbo; Kinematic model; Neural network optimization; Positioning error prediction

1 Introduction

Energy development and infrastructure construction are very important worldwide. The drilling-blasting method remains one of the primary techniques used in hard-rock roadway excavation (Sethu et al., 2017). Rock-drilling jumbos are the most widely used tunneling equipment in coal-energy exploitation and underground tunnel construction. Compared with traditional rock drills, the three-boom rock-drilling rig has the advantages of high mechanization and fast drilling speed, which can effectively improve drilling efficiency and reduce labor intensity for workers. The positioning accuracy of rock-drilling booms is an important factor affecting excavation efficiency and section-forming quality in the mining of roadways and engineering tunnels (Kahraman et al., 2006; Wang et al., 2015). The self-weight, strong coupling, complex structure, and long boom length of a three-boom drilling jumbo can easily cause excessive positioning error, which significantly hinders the efficiency of roadway excavation (Costamagna et al., 2018, 2021; Navarro et al., 2019; Tsagaris and Mansour, 2019). Therefore, accurate prediction and compensation of positioning error for the drilling mechanism of three-boom rock-drilling jumbos is key to improving drilling performance.

Many researchers have extensively investigated kinematic solutions. Köker (2013) combined a simulated annealing algorithm with a neural network to solve the kinematics, and confirmed the superiority of the proposed algorithm in the Puma 560 six-joint robot. Chen et al. (2014) introduced a kinematic analysis method for a multi-degree-of-freedom (multi-DOF) thumb robot, based on dual quaternions. Zhang and Hannaford (2019) developed a knowledge-based intelligent system that could solve closed inverse kinematics problems using behavior trees, imitating human

✉ Songyong LIU, lsycumt@163.com
Songyong LIU, https://orcid.org/0000-0002-2801-7969

Received Nov. 21, 2023; Revision accepted Feb. 14, 2024;
Crosschecked Oct. 31, 2024; Online first Jan. 13, 2025

expert behaviors. Jiang et al. (2017) resolved the inverse kinematics issue for a 6-DOF robot by utilizing a back-propagation (BP) neural network algorithm optimized by particle swarm optimization (PSO). Wu et al. (2021) combined the parametric method with a multi-objective evolutionary algorithm, and added a population migration strategy and an adaptive interval search operator to the algorithm. They demonstrated the effectiveness of their approach by using an 8-DOF tunnel shotcrete robot as an example to solve the inverse kinematics problem. To address the inverse kinematics problem in a 7-DOF manipulator, Zhang and Xiao (2019) incorporated chaotic mapping into the artificial bee colony (ABC) algorithm to avoid local optimization. Liu et al. (2021) enhanced the PSO algorithm by dynamically adjusting the inertia weight with a similarity method to address the inverse kinematics problem of manipulators that fail to meet the Pieper criterion. Wang et al. (2020) introduced a novel optimization method for inverse kinematics that used Gaussian damped least squares. Faster convergence of the algorithm was achieved by incorporating the optimal enhancement step coefficient. Neural networks have also been utilized in inverse kinematics, and offer the advantages of rapid convergence and reliable stability (Chiddarwar and Babu, 2010; Köker et al., 2014).

In recent years, there have been numerous studies examining the positioning error of different manipulators. Zeng et al. (2017) devised an error prediction model utilizing the linear unbiased optimal estimation technique, grounded in spatial similarity. Luo et al. (2021) developed a joint clearance-based error model, which predicts the positioning error for every joint position. The experimental findings illustrated that this technique was successful in reducing positioning errors. Chen et al. (2019) proposed a compensation method for position error in aviation drilling robots, which combined error similarity with a radial basis function (RBF) neural network. To enhance absolute position accuracy, Yuan et al. (2018) developed a compensation method based on an extreme learning optimization model. In order to improve the absolute position error of the manipulator in an automobile assembly line, Cao et al. (2019) examined a method that reduced the absolute position error of the robot using machine vision and a neural network. Du et al. (2021) introduced an online cognitive joint angle error compensation method based on incremental learning, to address the impact of the joint angle error of the manipulator on the precision of the end effector. Yu (2021) utilized a BP neural network, RBF neural network, and control module to mitigate non-geometric error in a parallel robot. The effectiveness of this approach was demonstrated by experimental results. Li B et al. (2022) developed an error compensation model for an industrial robot, utilizing a neural network optimized by the genetic particle swarm algorithm, resulting in improved positioning accuracy for the robot. These studies provide a theoretical foundation for the precision compensation of manipulators.

According to the existing research, the drilling accuracy of drilling jumbos has been limited to 10 cm for a long time, and the causes of inaccurate positioning of the drilling boom (such as shaft-hole clearance, friction, and flexibility) cannot be eliminated. Therefore, what we consider here is the effective simulation of various factors with neural network models to realize accurate compensation of the movement error of the drilling boom end position. The paper is structured as follows. Section 2 describes how we combined analytical and iterative methods to enhance the efficiency of the kinematics solution. Section 3 shows how we optimized the BP neural network using an improved sparrow search algorithm (ISSA), and established a positioning error prediction model for a three-boom rock-drilling jumbo. Section 4 presents the results of experimental positioning error compensation. Conclusions are drawn in Section 5.

2 Kinematics of multi-boom rock-drilling jumbos

According to field-drilling and blasting-excavation experience, tunnel-excavation quality depends on the quality of drilling holes, which are determined by the positioning accuracy of rock-drilling-jumbo drilling booms. For the drilling holes in the working face, the tilt angle of a peripheral hole can easily cause serious over-excavation or under-excavation of a tunnel, while the tilt angle of the cut hole will determine blasting efficiency. Therefore, it is necessary to accurately draw the centerline and contour line of the excavation section and mark the drilling position. Then, the rock-drilling jumbo must be positioned at a certain distance from the working face and the centerline of the jumbo kept stable and parallel to the tunnel axis, to ensure that

the drilling boom is able to reach the target drilling hole in each area of the working face at an appropriate tilt angle.

2.1 Mathematical model of kinematics

The boom structure of a three-boom rock-drilling jumbo comprises five rotating joints and two moving joints, which provide seven DOFs, as illustrated in Fig. 1. To study the kinematic features of a three-boom rock-drilling jumbo, we established a kinematic model of the boom utilizing the modified Denavit-Hartenberg (D-H) method (Zhang et al., 2014).

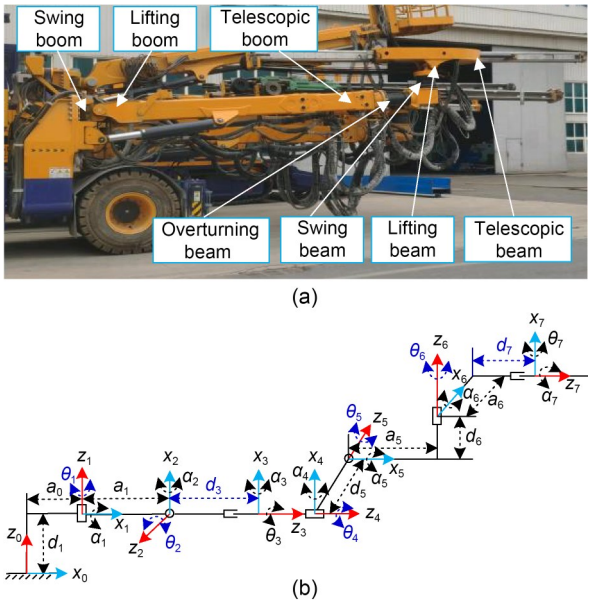

Fig. 1 Structure and kinematics model of a drilling boom: (a) drilling boom structure of a rock-drilling jumbo; (b) kinematics model of a rock-drilling boom

According to the principle of coordinate transformation, the D-H parameter table of each boom is obtained as shown in Table 1. θ_i, d_i, a_{i-1}, and α_{i-1} represent the rotation angle from x_{i-1} to x_i around the z_i axis, the translation distance from x_{i-1} to x_i along the z_i axis, the translation distance from z_{i-1} to z_i along the x_{i-1} axis, and the rotation angle from z_{i-1} to z_i around the x_{i-1} axis, respectively.

Table 1 D-H parameters of a drilling jumbo

i	α_{i-1} (°)	a_{i-1} (mm)	θ_i (°)	d_i (mm)	Variable
1	0	195	(−42, 42)	50	θ_1
2	90	150	(−145, 48)	0	θ_2
3	90	0	0	(5598, 8098)	d_3
4	0	0	(−190, 190)	0	θ_4
5	90	0	(−100, 280)	661	θ_5
6	90	60	(60, 135)	614	θ_6
7	90	245.5	90	(4022, 5822)	d_7

Therefore, the transformation matrix for the joint pose between the adjacent coordinate systems i and $i-1$ can be presented as

$$ {}^{i-1}_{i}\boldsymbol{T}=\begin{bmatrix} c\theta_i & -s\theta_i & 0 & a_{i-1} \\ s\theta_i c\alpha_{i-1} & c\theta_i c\alpha_{i-1} & -s\alpha_{i-1} & -d_i s\alpha_{i-1} \\ s\theta_i s\alpha_{i-1} & c\theta_i s\alpha_i & c\alpha_{i-1} & d_i c\alpha_{i-1} \\ 0 & 0 & 0 & 1 \end{bmatrix}, \quad (1) $$

where $c\theta_i$, $s\theta_i$, $c\alpha_{i-1}$, and $s\alpha_{i-1}$ denote $\cos\theta_i$, $\sin\theta_i$, $\cos\alpha_{i-1}$, and $\sin\alpha_{i-1}$, respectively. The overall transformation matrix of a drilling boom is shown as

$$ {}^{0}_{7}\boldsymbol{T}={}^{0}_{1}\boldsymbol{T}\,{}^{1}_{2}\boldsymbol{T}\,{}^{2}_{3}\boldsymbol{T}\,{}^{3}_{4}\boldsymbol{T}\,{}^{4}_{5}\boldsymbol{T}\,{}^{5}_{6}\boldsymbol{T}\,{}^{6}_{7}\boldsymbol{T}=\begin{bmatrix} n_x & o_x & a_x & p_x \\ n_y & o_y & a_y & p_y \\ n_z & o_z & a_z & p_z \\ 0 & 0 & 0 & 1 \end{bmatrix}, \quad (2) $$

where $\boldsymbol{n}=[n_x, n_y, n_z]^{\mathrm{T}}$, $\boldsymbol{o}=[o_x, o_y, o_z]^{\mathrm{T}}$, and $\boldsymbol{a}=[a_x, a_y, a_z]^{\mathrm{T}}$ are the direction vectors of the coordinate system at the end of the drilling boom in the base coordinate system. $\boldsymbol{p}=[p_x, p_y, p_z]^{\mathrm{T}}$ is the position vector of the coordinate system at the end of the drilling boom in the base coordinate system.

2.2 Inverse kinematics solutions for different working conditions

The 7-DOF manipulator of a three-boom drilling jumbo functions as a drilling boom. Though it possesses high flexibility and can efficiently navigate obstacles in space, it presents challenges in terms of solving the inverse kinematics. Currently, the two primary methods for resolving reverse kinematics include the analytical and iterative methods. While the analytical method can produce quick and precise results, it can only solve inverse kinematics if the manipulator structure satisfies Pieper's criterion (Raghavan and Roth, 1993). The iterative method is appropriate when there is no analytical solution, but it relies heavily on the initial value and is time-consuming.

Blast holes can be categorized as cut holes, auxiliary holes, or peripheral holes, based on their function. Fig. 2 displays the drilling hole layout diagram for a tunnel.

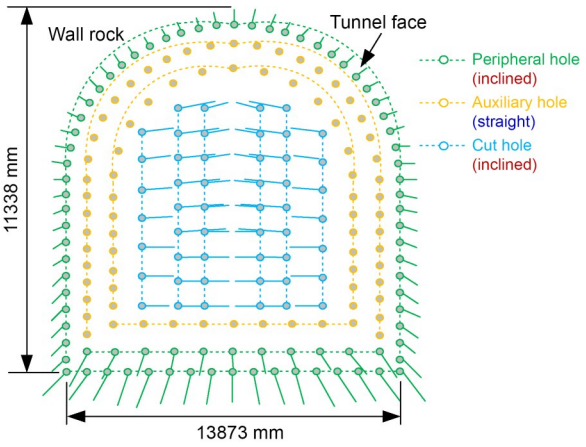

Fig. 2 Drilling hole layout diagram for a tunnel. References to color refer to the online version of this figure

When drilling various boreholes, the necessary positioning of the drilling boom also varies. For instance, when drilling auxiliary holes, it is crucial to position the drilling boom perpendicular to the tunnel face. We propose a new combinatorial calculation method designed to eliminate the waste of time and hardware resources caused by iterating all drilling holes. We adopted analytical methods to solve straight-hole conditions, and iterative methods to address the working conditions for inclined holes.

2.2.1 Analysis of straight-hole conditions

The inverse kinematics analysis is conducted with the drilling boom oriented perpendicular to the working face. According to the operator's habit, the rolling angle is divided into 0° and 180° for discussion. It can be seen from Fig. 1 that the end joint d_7 is a moving joint. After the values are determined for all six joints, d_7 only needs to move on its axis. Therefore, d_7 can be regarded as a constant here to reduce computational complexity. The right side of Eq. (3) follows the chain multiplication criterion of the forward kinematics approach.

$$\begin{bmatrix} c\theta_1 & s\theta_1 & 0 & -a_0c\theta_1 \\ -s\theta_1 & c\theta_1 & 0 & a_0s\theta_1 \\ 0 & 0 & 1 & -d_1 \\ 0 & 0 & 0 & 1 \end{bmatrix} \begin{bmatrix} n_x & o_x & a_x & p_x \\ n_y & o_y & a_y & p_y \\ n_z & o_z & a_z & p_z \\ 0 & 0 & 0 & 1 \end{bmatrix} = {}^1_2\boldsymbol{T}\,{}^2_3\boldsymbol{T}\,{}^3_4\boldsymbol{T}\,{}^4_5\boldsymbol{T}\,{}^5_6\boldsymbol{T}\,{}^6_7\boldsymbol{T}. \tag{3}$$

The equation is expanded and simplified based on the various positions of the drilling boom.

Case 1. When the roll angle is 0°, the constraint can be obtained: $\theta_2+\theta_5=0°$, $\theta_1+\theta_6=90°$, and $\theta_4=0°$.

Make the elements at (2, 4) positions on both sides of the matrix equal:

$$(p_y-a_6)c\theta_1+(a_0-p_x+d_7)s\theta_1=d_5. \tag{4}$$

After trigonometric transformation of Eq. (4),

$$\theta_1=\arcsin\left(\frac{d_5}{\sqrt{(p_y-a_6)^2+(a_0-p_x+d_7)^2}}\right)-\arctan\left(\frac{p_y-a_6}{a_0-p_x+d_7}\right). \tag{5}$$

Therefore, $\theta_6=90°-\theta_1$.

Make the elements (1, 4) and (3, 4) on both sides of the matrix equal. Set $L_1=(p_x-a_0-d_7)c\theta_1+(p_y-a_6)s\theta_1-a_1-a_5$ and $L_2=p_z-d_1-d_6$. Therefore,

$$\begin{cases} a_2c\theta_2-d_3s\theta_2=L_1, \\ -a_2s\theta_2-d_3c\theta_2=L_2. \end{cases} \tag{6}$$

Add the squares of both ends of Eq. (6):

$$d_3=\sqrt{L_1^2+L_2^2-a_2^2}. \tag{7}$$

After trigonometric transformation of Eq. (7),

$$\theta_2=\operatorname{atan2}(-L_2,\ L_1)-\operatorname{atan2}(d_3,\ a_2). \tag{8}$$

Therefore, $\theta_5=-\theta_2$.

Case 2. When the roll angle is 180°, the constraints can be obtained: $\theta_2-\theta_5=-180°$, $\theta_1-\theta_6=-90°$, and $\theta_4=180°$.

Make the elements at (2, 4) positions on both sides of the matrix equal:

$$(p_y+a_6)c\theta_1+(a_0-p_x+d_7)s\theta_1=-d_5. \tag{9}$$

After trigonometric transformation of Eq. (9),

$$\theta_1=\arcsin\left(\frac{-d_5}{\sqrt{(p_y+a_6)^2+(a_0-p_x+d_7)^2}}\right)-\arctan\left(\frac{p_y+a_6}{a_0-p_x+d_7}\right). \tag{10}$$

Therefore, $\theta_6=90°+\theta_1$.

Make the elements (1, 4) and (3, 4) on both sides of the matrix equal. Set $L_3=(p_x-a_0-d_7)c\theta_1+(p_y+a_6)s\theta_1-a_1-a_5$ and $L_4=p_z-d_1+d_6$. Therefore,

$$\begin{cases} a_2c\theta_2-d_3s\theta_2=L_3, \\ -a_2s\theta_2-d_3c\theta_2=L_4. \end{cases} \tag{11}$$

Add the squares of both ends of Eq. (11):

$$d_3=\sqrt{L_3^2+L_4^2-a_2^2}. \tag{12}$$

After trigonometric transformation of Eq. (12),

$$\theta_2=\text{atan2}(-L_4,\ L_3)-\text{atan2}(d_3,\ a_2). \tag{13}$$

Therefore, $\theta_5=\theta_2+180°$.

All of the formulas for inverse kinematics have been acquired.

2.2.2 Analysis of inclined-hole conditions

In general, a drilling boom has the capability to reach the blast hole in any position, while each joint is unconstrained. However, the analytical method cannot be utilized when the drilling boom does not satisfy Pieper's criterion. In this case, only the iterative method can solve the inverse kinematics. The *ZYX* Euler angle shown in Fig. 3 can be implemented in Eq. (14) to express the attitude angles of the object.

$$\begin{cases} \beta=\text{atan2}\left(-n_z,\ \sqrt{n_x^2+n_y^2}\right), \\ \alpha=\text{atan2}\left(\dfrac{n_y}{\cos\beta},\ \dfrac{n_x}{\cos\beta}\right), \\ \gamma=\text{atan2}\left(\dfrac{o_z}{\cos\beta},\ \dfrac{a_z}{\cos\beta}\right). \end{cases} \tag{14}$$

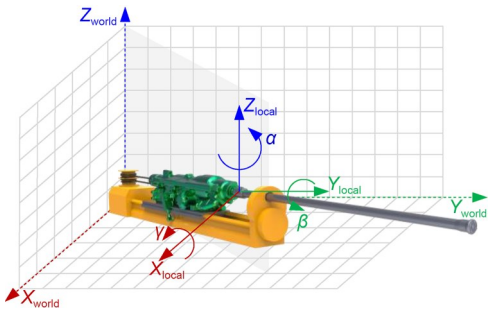

Fig. 3 Blast-hole layout diagram of a tunnel

The object has three attitude equations and three position equations in space, so there are six nonlinear equations in total. Set $\boldsymbol{f}=[f(1), f(2), f(3), f(4), f(5), f(6)]^{\mathrm{T}}$.

$$\boldsymbol{f}=\begin{cases} f(1)={}_7^0T(1,\ 4)-p_x, \\ f(2)={}_7^0T(2,\ 4)-p_y, \\ f(3)={}_7^0T(3,\ 4)-p_z, \\ f(4)=\text{atan2}\left(-{}_7^0T(3,\ 1),\ \sqrt{{}_7^0T(1,\ 1)^2+{}_7^0T(2,\ 1)^2}\right)-\beta, \\ f(5)=\text{atan2}\left(\dfrac{{}_7^0T(2,\ 1)}{\cos\beta},\ \dfrac{{}_7^0T(1,\ 1)}{\cos\beta}\right)-\alpha, \\ f(6)=\text{atan2}\left(\dfrac{{}_7^0T(3,\ 2)}{\cos\beta},\ \dfrac{{}_7^0T(3,\ 3)}{\cos\beta}\right)-\gamma, \end{cases} \tag{15}$$

where ${}_7^0T(i, j)$ represents the element of row i and column j in the pose matrix. In summary, solving a set of complex nonlinear equations is key to solving inverse kinematics. PSO has become widely accepted due to its high accuracy and quick convergence (Liu et al., 2007; Li et al., 2012). In light of the challenge posed by selecting the initial point of the conventional numerical algorithm, we employ the PSO algorithm to obtain the search point, which is then allocated to the global search algorithm to solve the inverse kinematics equation. The solution steps are shown in Table 2.

Table 2 Steps for solving inverse kinematics. c_1 and c_2 are learning factors, and n_{r1} and n_{r2} are random numbers between 0 and 1

Input: position and attitude matrix (***T***), population (p), iteration times (t), inertia factor (w), objective function (f)
Output: joint variables (θ_1, θ_2, d_3, θ_4, θ_5, θ_6)
Step 1: Determine the initial position x_i and its velocity v_i.
Step 2: Calculate particle fitness and update individual extremum (p_{best}) and global extremum (g_{best}).
Step 3: Update particle velocity: $v_i=wv_i+c_1n_{r1}(p_{\text{best},i}-x_i)+c_2n_{r2}(g_{\text{best},i}-x_i)$. Update particle position: $x_i=x_i+v_i$.
Step 4: Output search points after iteration.
Step 5: Use global search to solve the equation at a given initial point.
Step 6: Global search algorithm generates test points, initializes thresholds and counters, and starts the main loop.
Step 7: Output the result when the end condition is met.

In order to verify the effectiveness of the PSO combined with the global search algorithm, we first randomly generated a series of joint displacements and angles within the moving range of each joint, as the inputs of the algorithm. They also served as a reference for the accuracy of the inverse kinematics solution of the drilling boom. The corresponding end position of the drilling boom was obtained from the displacements and angles of each joint through the forward kinematics model. PSO was used in combination with a global search algorithm to find the inverse solutions corresponding to the generated end position of the drilling boom, which was taken as the estimated value of every joint. We randomly selected and verified 550 sets of data to validate the algorithm's accuracy. The input consisted of the drilling boom's position and attitude at the end, while the output included the joint variables. By comparing the estimated values with the true values of the joints generated randomly, we were able to obtain the inverse kinematics solution error of each joint, as shown in Fig. 4a; Fig. 4b presents the comparison between the simulated inverse kinematic values and the true values of joint 1.

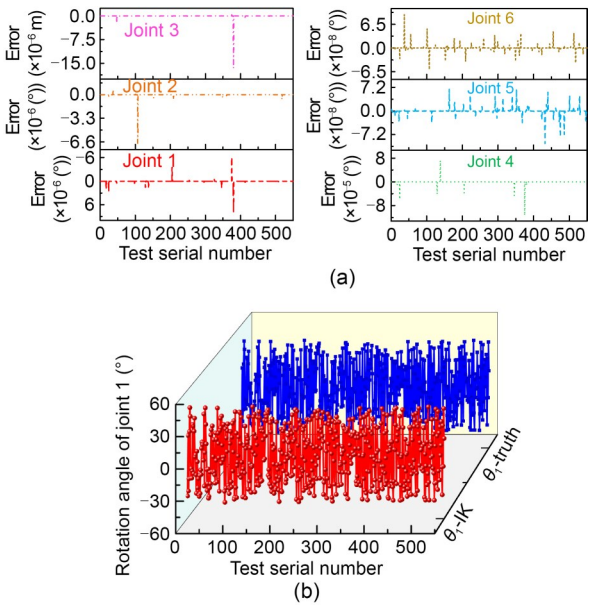

Fig. 4 Inverse kinematic solution results for each joint: (a) inverse kinematic error of each joint; (b) inverse kinematic (IK) values and true values of joint 1

The test data in Fig. 4 shows that the maximum angle error of the rotating joint was within 1.13×10^{-4}° and the maximum error of the moving joint was within 1.65×10^{-5} m. These results indicate that the overall calculation error was small, meeting the accuracy requirements of the actual control system.

3 Positioning error compensation method

3.1 Modeling of BP neural network optimized by an ISSA

There are numerous factors that contribute to the positioning error of a drilling boom's end, such as assembly and flexibility errors. Establishing an error model is challenging due to these factors. Meanwhile, neural networks possess excellent nonlinear data-fitting capabilities and can acquire input–output mapping through trained samples (Ahmadi et al., 2014; Goetzke-Pala et al., 2018). Several studies have shown that double-layer networks have a better ability to deal with nonlinear data compared to single-hidden-layer networks. Therefore, for the purpose of establishing an error prediction model of a three-boom rock-drilling jumbo, we chose to use a double-hidden-layer neural network, shown in Fig. 5. The anticipated coordinate (x, y, z) of the drilling boom serves as the input, while the positioning error $(\Delta x, \Delta y, \Delta z)$ is the output.

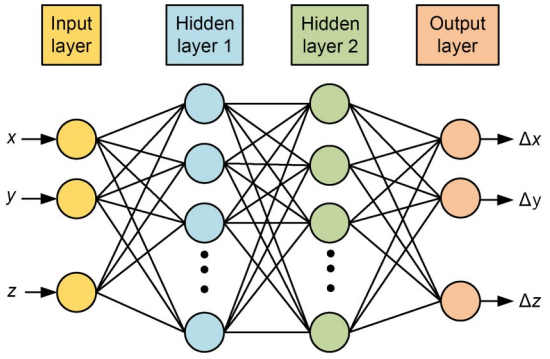

Fig. 5 Structure of double-hidden-layer neural network

In neural network modeling, the choice of weights and thresholds will directly affect the prediction accuracy of the training model and can result in excessively long network training time. In order to quickly obtain the optimal weights and thresholds for our neural network and improve the training efficiency and prediction accuracy of the algorithm, we optimized a BP neural network by incorporating a sparrow search algorithm. A sparrow search algorithm is a swarm intelligence optimization algorithm based on the behavior of sparrows foraging and avoiding predators. The initial

sparrow population is defined as either producers or scroungers. The producers usually have high energy reserves, and are responsible for determining the areas where rich food sources can be found and providing foraging areas or directions for the whole sparrow population. Other individuals, the scroungers, follow the producers who provide the best food to find food. At the same time, a certain proportion of individuals in the population are responsible for investigation and early warning (scouts). Once predator danger is detected, they will give up their current food and position and quickly move to a safe area around producers. During foraging periods, every sparrow has only one attribute: position. There are three possible behaviors in the iterative change of each sparrow's position: (1) continue to search for food as a producer; (2) monitor and follow a producer for food as a scrounger; (3) alert for predator danger as a scout and move to a safer area around producers (Song et al., 2021; Li XY et al., 2022; Li ZL et al., 2022).

During the search process, producers obtain food first and provide guidance to all scroungers on food location. The formula for updating producer location is as follows:

$$x_{ij}^{t+1}=\begin{cases}x_{ij}^{t}\cdot\exp\left(\dfrac{-i}{a\cdot n_{\text{it, max}}}\right), & R<S,\\ x_{ij}^{t}+Q\cdot\boldsymbol{L}, & R\geq S,\end{cases}\tag{16}$$

where t represents the current number of iterations, $\boldsymbol{L}$ represents a matrix with dimensions of $1\times d$ (d is the dimension of the optimization problem, i.e., the initial weight and threshold of the neural network), $n_{\text{it, max}}$ is the maximum number of iterations, Q is a random number of normal distribution, x_{ij} is the position of the ith sparrow in the jth dimension, and a is a random number between 0 and 1. R and S are warning and safety values, respectively. When $R<S$, which means that there are no predators around, the producer enters the wide search mode. When $R\geqslant S$, it means that some sparrows have discovered a predator, and all sparrows need to quickly fly to safe areas.

The location of a scrounger is updated as:

$$x_{ij}^{t+1}=\begin{cases}Q\cdot\exp\left(\dfrac{x_{\text{wj}}^{t}-x_{ij}^{t}}{\alpha\cdot n_{\text{it, max}}}\right), & i>\dfrac{n}{2},\\ x_{\text{p}}^{t+1}+|x_{ij}^{t}-x_{\text{pj}}^{t+1}|\boldsymbol{M}^{+}\boldsymbol{L}, & \text{other},\end{cases}\tag{17}$$

where x_{pj} and x_{wj} are the best and worst positions for the provider, respectively. $\boldsymbol{M}$ is a 1-row d-column matrix with a random value of 1 or −1 for each element, and $\boldsymbol{M}^{+}=\boldsymbol{M}^{\text{T}}(\boldsymbol{M}\boldsymbol{M}^{\text{T}})^{-1}$. n is the number of sparrows. When $i>n/2$, it suggests that the ith scrounger with the worse fitness value is most likely to be starving.

The sparrows who perform reconnaissance are called scouts. If danger arises, they abandon their food. The scout-position update formula is as follows:

$$x_{ij}^{t+1}=\begin{cases}x_{\text{bj}}^{t}+\xi\cdot|x_{ij}^{t}-x_{\text{bj}}^{t}|, & f_i>f_{\text{g}},\\ x_{ij}^{t}+K\cdot\dfrac{|x_{ij}^{t}-x_{\text{bj}}^{t}|}{(f_i-f_{\text{w}})+\varepsilon}, & f_i=f_{\text{g}},\end{cases}\tag{18}$$

where K is a random number of $[-1, 1]$ and denotes the direction in which the scout sparrow moves; ξ is the step size; x_{bj} represents the current global best position; ε represents a small constant; f_{w}, f_{g}, and f_i represent the global worst, global best, and individual fitness of the current sparrow, respectively. For simplicity, when $f_i>f_{\text{g}}$, it indicates that the sparrow is at the edge of the group. X_{best} represents the location of the center of the population and the safe area around it. $f_i=f_{\text{g}}$ shows that the sparrows in the middle of the population are aware of the danger and need to move closer to the others.

Because the individual method of the sparrow search algorithm for obtaining the optimal solution involves jumping in the near vicinity of the current optimal solution, its global search capability is limited, and it tends to be confined to the local optimal solution. Therefore, we decided to try decreasing the jump to the optimal position and moving directly to the optimal position instead. We modified the finder location update formula as follows:

$$x_{ij}^{t+1}=\begin{cases}x_{ij}^{t}\cdot(1+Q), & R<S,\\ x_{ij}^{t}+Q, & R\geq S.\end{cases}\tag{19}$$

Then, we changed the formula for updating participant location to the following:

$$x_{ij}^{t+1}=\begin{cases}Q\cdot\exp\left(\dfrac{x_{\text{wj}}^{t}-x_{ij}^{t}}{i^{2}}\right), & i>\dfrac{n}{2},\\ x_{\text{pj}}^{t}+|x_{\text{pj}}^{t}-x_{ij}^{t}|\cdot\text{rand}(0, 1), & \text{other}.\end{cases}\tag{20}$$

The optimized process for the BP neural network, using the ISSA, is illustrated in Fig. 6, and the specific steps are depicted in Table 3.

3.2 Training and verification of the neural network

The training and test datasets of the optimized neural network were acquired by a total station in the field experiment shown in Fig. 7. The drilling booms of a three-arm rock-drilling jumbo were derived to simulate drilling holes at 1124 positions. Therefore, 1124 sets of sample data were collected in the positioning experiment. The 1124 sample data groups were divided into three sections to train, test, and verify the proposed model in Section 3.1. Among them, 1000 sets were used for training, 100 sets for testing, and 24 sets for verification. Prior to neural network training, the sample data were normalized and projected to [0, 1] after linearization, to avoid singular values. The conversion function is displayed in Eq. (21).

$$\boldsymbol{P}'_{[i]}=\frac{\boldsymbol{P}_{[i]}-\boldsymbol{P}_{[i]\min}}{\boldsymbol{P}_{[i]\max}-\boldsymbol{P}_{[i]\min}},\quad i=1,\ 2,\ 3, \tag{21}$$

where $\boldsymbol{P}_{[i]}$ is the non-normalized input matrix, and $\boldsymbol{P}'_{[i]}$ is the normalized input matrix.

Subsequently, the BP neural network parameters were established, and the number of nodes in the hidden layer l was determined based on

$$l=\sqrt{m+N}+a, \tag{22}$$

where m, N, and a are the number of nodes in the input layer, the number of nodes in the output layer, and a constant between 1 and 10, respectively.

Thus, both hidden layers contained seven nodes, with a learning rate of 0.01. The training error was set at 1×10^{-4}, and training concluded once the stop condition was met. We saved the prediction model after training and input 24 groups of theoretical points from the verification set. Using the saved model, we predicted the positioning error before comparing it with the total station measurement results. Fig. 8a primarily shows the predicted and the actual 3D coordinate error of the end point of the drilling boom, while the 3D coordinate error of the predicted position of the drilling boom relative to the actual position is shown in Fig. 8b.

Table 4 presents a comparison of the prediction outcomes of the proposed BP neural network optimized by the ISSA (ISSA-BP) with those of the original BP neural network. It is evident that the greatest forecast errors in the X, Y, and Z directions decreased by 22.9%, 38.2%, and 39.1%, respectively. In the validation data, the optimized neural network model demonstrates higher prediction accuracy and stability, as evidenced by a maximum deviation of 1.71 cm, a maximum standard deviation of 0.49 cm, and an accuracy of 81.7%.

4 Error compensation experiment

4.1 Experimental arrangement

The principle of the compensation method for drilling boom positioning error using a neural network is illustrated in Fig. 9. Initially, a sampling point P is planned within the workspace. The actual position is then measured using a total station, and the positioning error E for the drilling boom is obtained. It is then included in the training of the neural network model to predict the positioning error E_{d} of the ideal point. Finally, the positioning error of the predicted value is added to the theoretical coordinate P_{desired} of the target

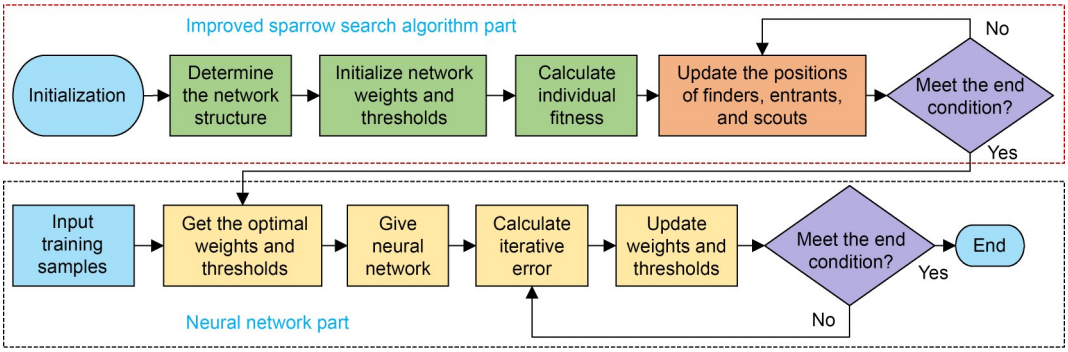

Fig. 6 Process of BP neural network optimized by the ISSA

Table 3 Steps of BP neural network optimized by the ISSA. *o* is the predicted output, and *r* is the expected output

Input: training data; number of hidden layer nodes (h_1, h_2), number of input layer nodes (m), number of output layer nodes (N), maximum evolutionary algebra (G_{max}), population (p), Alboom value (R_A)
Output: the best individual (F_{best})
Step 1: Initialize the network structure.
Step 2: Establish the function of fitness: $F(i)=\dfrac{1}{\frac{1}{2}\sum_{i=1}^{N}(o_i-r_i)^2}$.
Step 3: Rank individual sparrows according to fitness function values.
Step 4: Update provider, scrounger, and scout locations.
Step 5: Calculate fitness and update position.
Step 6: Cycle through steps 3 to 5 to get the best individual (F_{best}).
Step 7: The optimal weights and thresholds obtained by the ISSA are given to the network.

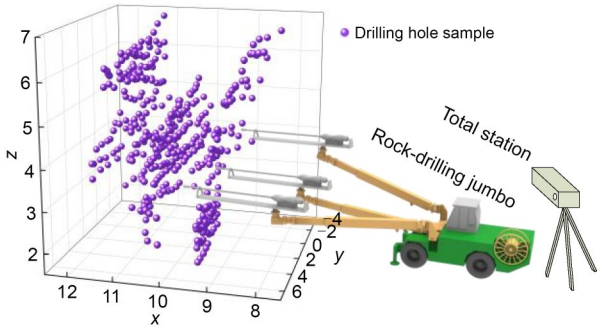

Fig. 7 Positioning experiment schematic of drilling booms of a three-arm rock-drilling jumbo

point to obtain the modified target point $P_{modified}$ for compensation.

This study focuses on conducting an error compensation experiment on a three-boom rock-drilling jumbo. Fig. 10 shows the experimental process of error compensation, with IK representing the inverse kinematics solution. First, the layout planning for the borehole is conducted within the workspace of the rock-drilling jumbo, and the target position is chosen to establish a simulated tunnel face. Once the target position is resolved, the drilling boom is operated to carry out the initial positioning of all points. Subsequently, the anticipated point position is inputted into the trained neural network model to forecast positioning inaccuracy. The anticipated error is corrected for the intended point, and then the inverse kinematics is solved again to acquire the values for every joint variable. Afterward, the revised joint variable is used as the input for the control system of the jumbo, and it drives each drilling boom joint to its corresponding position for the completion of secondary positioning, thus achieving error compensation.

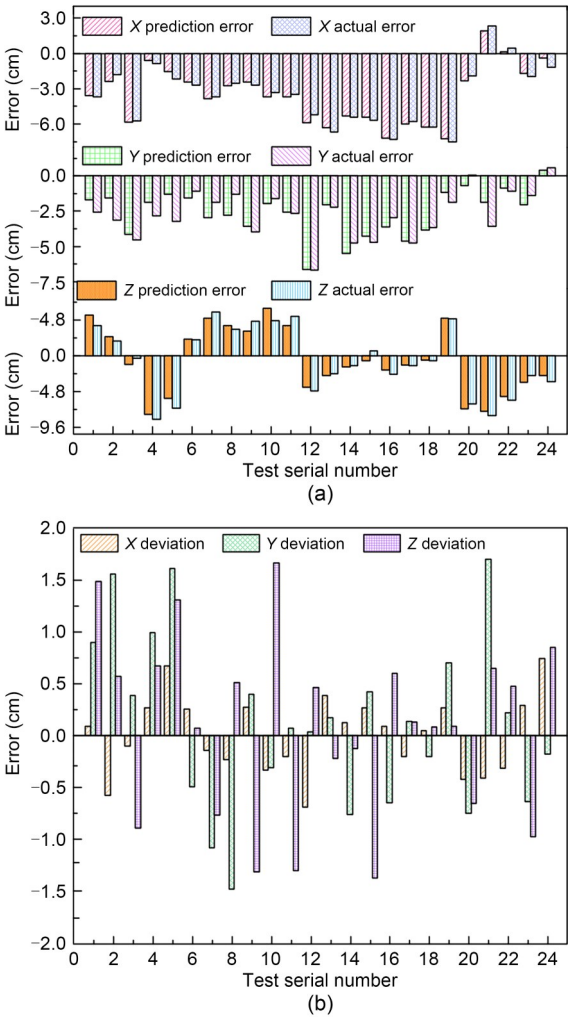

Fig. 8 Prediction result and deviation of the neural network: (a) prediction result; (b) prediction deviation

Table 4 Comparison of prediction deviation results

Model	Direction	Deviation (cm)		
		Max	Mean	Standard
BP	*X*	0.96	0.34	0.28
	Y	2.77	0.76	0.81
	Z	2.73	0.72	0.58
ISSA-BP	*X*	0.74	0.31	0.19
	Y	1.71	0.70	0.49
	Z	1.66	0.65	0.47

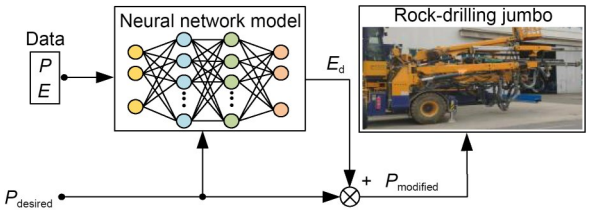

Fig. 9 Positioning error compensation principle of a drilling boom

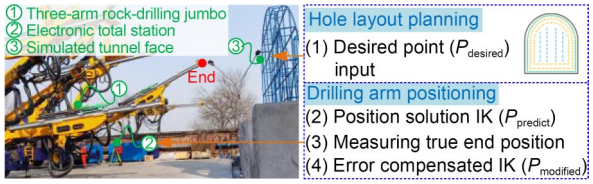

Fig. 10 Experimental positioning error compensation process for a drilling boom

4.2 Experimental results

Based on the above process, we selected 10 anticipated coordinate points in the working space of the jumbo to verify the effectiveness of the compensation method. Of these, points No. 1, No. 2, No. 3, No. 6, and No. 7 were inclined drilling holes, while points No. 4, No. 5, No. 8, No. 9, and No. 10 were straight drilling holes. The total station was used to measure the end position of the drilling boom multiple times before and after the compensation experiment, and the measured coordinate position distribution was projected on the plane, as shown in Fig. 11a. The error comparison between the actual position and the theoretical position of the drilling boom end before and after the compensation experiment is given in Fig. 11b.

Fig. 11 reveals that borehole positioning error was substantially reduced after compensation. The accuracy of drilling holes No. 4 and No. 5, which were at the top of the simulated tunnel, was relatively low due to the large elongation and elevation of the drilling boom at the top, and due to the presence of flexible error and under-damping in the mechanism adjustment. The maximum position error before compensation was 10.94 cm, and after compensation, it was reduced to 7.51 cm. The average error decreased from 9.79 to 5.92 cm, resulting in a 39.5% reduction in error. This indicates that the error compensation model put forward in this paper can significantly enhance the drilling-positioning accuracy of a three-boom rock-drilling jumbo.

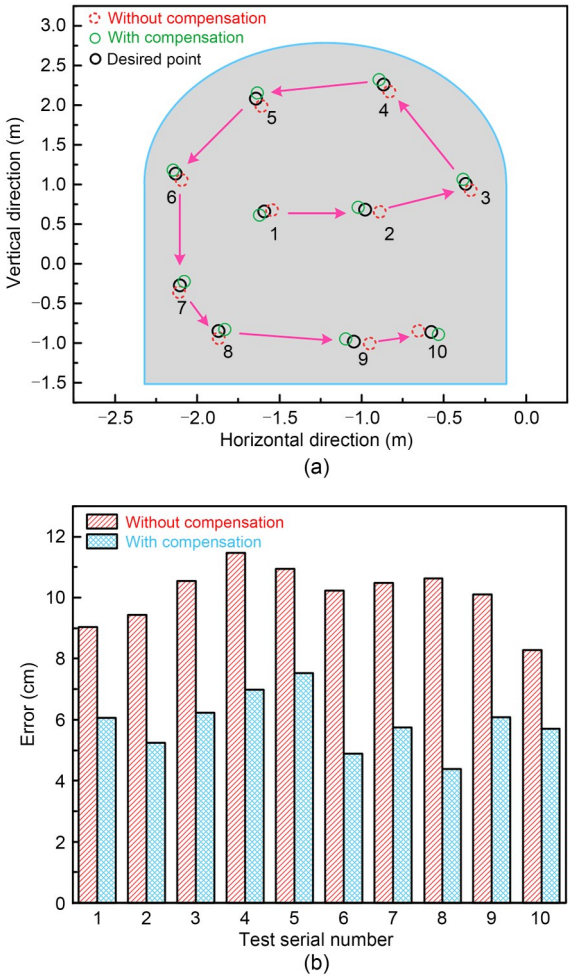

Fig. 11 Comparison of the drilling boom positioning error with and without compensation: (a) drilling hole distribution; (b) positioning error

5 Conclusions

In this study, we examined the drilling-positioning error of a multi-boom rock-drilling jumbo. The research findings offer a valuable reference for the automation of roadway excavation. Key findings show that:

(1) To solve the point position under working conditions of an inclined hole for the drilling boom of the three-boom rock-drilling rig that does not meet the Pieper criterion, we derived an inverse kinematics formula for straight-hole conditions through analytical methods. Subsequently, we used a global search algorithm. The simulation findings indicate that the maximum angle error in the rotational joint is less than 1.13×10^{-4}°, and the maximum error in the motion joint is less than 1.65×10^{-5} m. A small calculation error was

observed, which meets the accuracy requirements of the control system in practice.

(2) We established an error prediction model using a BP neural network optimized by an ISSA. The model's prediction reliability is confirmed. The findings demonstrate a maximum prediction error and standard deviation of 1.71 and 0.49 cm, respectively. With a prediction accuracy of 81.7%, the neural network model exhibits high prediction accuracy and stability.

(3) Additionally, the error prediction model outputs the positioning error and compensates it to the desired point for an inverse solution, serving as the control system's input. The experimental findings demonstrate a 39.5% reduction in average positioning error, from 9.79 to 5.92 cm. Moreover, the cumulative distance error of each test point is under 10 cm, fulfilling the actual positioning needs.

It is worth noting that although we greatly improved the positioning accuracy of the drilling boom in this study, the model is proposed specifically for the conventional hole-drilling conditions described here. In the near future, we will investigate the positioning error prediction and compensation for drilling booms in situations that involve bench drilling, secondary drilling, and drilling deviation caused by rock cracks.

Acknowledgments

This work is supported by the National Natural Science Foundation of China (No. 12472038), the Natural Science Foundation of Jiangsu Province (No. BK20230688), the Natural Science Foundation of the Jiangsu Higher Education Institutions of China (No. 22KJB440004), the Key Research and Development Program of Xuzhou (No. KC22404), and the Research Fund for Doctoral Degree Teachers of Jiangsu Normal University of China (No. 22XFRS011).

Author contributions

Yuming CUI wrote the first draft of the manuscript. Songyong LIU designed the research and helped to organize the manuscript. Zhengqiang SHU and Zhenli LV processed the corresponding data. Yuming CUI and Lie LI revised and edited the final version.

Conflict of interest

Yuming CUI, Songyong LIU, Zhengqiang SHU, Zhenli LV, and Lie LI declare that they have no conflict of interest.

References

Ahmadi M, Naderpour H, Kheyroddin A, 2014. Utilization of artificial neural networks to prediction of the capacity of CCFT short columns subject to short term axial load. *Archives of Civil and Mechanical Engineering*, 14(3): 510-517. https://doi.org/10.1016/j.acme.2014.01.006

Cao CT, Do VP, Lee BR, 2019. A novel indirect calibration approach for robot positioning error compensation based on neural network and hand-eye vision. *Applied Sciences*, 9(9):1940. https://doi.org/10.3390/app9091940

Chen DD, Wang TM, Yuan PJ, et al., 2019. A positional error compensation method for industrial robots combining error similarity and radial basis function neural network. *Measurement Science and Technology*, 30(12):125010. https://doi.org/10.1088/1361-6501/ab3311

Chen JB, Han D, Nie H, et al., 2014. Dual quaternion-based inverse kinematics of dexterous finger. *Journal of Vibroengineering*, 16(6):2813-2820.

Chiddarwar SS, Babu NR, 2010. Comparison of RBF and MLP neural networks to solve inverse kinematic problem for 6R serial robot by a fusion approach. *Engineering Applications of Artificial Intelligence*, 23(7):1083-1092. https://doi.org/10.1016/j.engappai.2010.01.028

Costamagna E, Oggeri C, Segarra P, et al., 2018. Assessment of contour profile quality in D&B tunnelling. *Tunnelling and Underground Space Technology*, 75:67-80. https://doi.org/10.1016/j.tust.2018.02.007

Costamagna E, Oggeri C, Vinai R, 2021. Damage and contour quality in rock excavations for quarrying and tunnelling: assessment for properties and solutions for stability. *IOP Conference Series: Earth and Environmental Science*, 833(1):012137. https://doi.org/10.1088/1755-1315/833/1/012137

Du GL, Liang YH, Gao BY, et al., 2021. A cognitive joint angle compensation system based on self-feedback fuzzy neural network with incremental learning. *IEEE Transactions on Industrial Informatics*, 17(4):2928-2937. https://doi.org/10.1109/Tii.2020.3003940

Goetzke-Pala A, Hoła A, Sadowski Ł, 2018. A non-destructive method of the evaluation of the moisture in saline brick walls using artificial neural networks. *Archives of Civil and Mechanical Engineering*, 18(4):1729-1742. https://doi.org/10.1016/j.acme.2018.07.004

Jiang GW, Luo MZ, Bai KQ, et al., 2017. A precise positioning method for a puncture robot based on a PSO-optimized BP neural network algorithm. *Applied Sciences*, 7(10):969. https://doi.org/10.3390/app7100969

Kahraman S, Ipek M, Guleryuz U, et al., 2006. Performance prediction of a jumbo drill in Pozanti–Ankara motorway tunnel (Turkey). *Tunnelling and Underground Space Technology*, 21(3-4):265. https://doi.org/10.1016/j.tust.2005.12.126

Köker R, 2013. A neuro-simulated annealing approach to the inverse kinematics solution of redundant robotic manipulators. *Engineering with Computers*, 29(4):507-515. https://doi.org/10.1007/s00366-012-0277-7

Köker R, Çakar T, Sari Y, 2014. A neural-network committee machine approach to the inverse kinematics problem solution of robotic manipulators. *Engineering with Computers*,

30(4):641-649.
https://doi.org/10.1007/s00366-013-0313-2

Li B, Tian W, Zhang CF, et al., 2022. Positioning error compensation of an industrial robot using neural networks and experimental study. *Chinese Journal of Aeronautics*, 35(2):346-360.
https://doi.org/10.1016/j.cja.2021.03.027

Li CH, Yang SX, Nguyen TT, 2012. A self-learning particle swarm optimizer for global optimization problems. *IEEE Transactions on Systems, Man, and Cybernetics, Part B (Cybernetics)*, 42(3):627-646.
https://doi.org/10.1109/Tsmcb.2011.2171946

Li XY, Li SB, Zhou P, et al., 2022. Forecasting network interface flow using a broad learning system based on the sparrow search algorithm. *Entropy*, 24(4):478.
https://doi.org/10.3390/e24040478

Li ZL, Zhu B, Dai Y, et al., 2022. Thermal error modeling of motorized spindle based on Elman neural network optimized by sparrow search algorithm. *The International Journal of Advanced Manufacturing Technology*, 121(1-2):349-366.
https://doi.org/10.1007/s00170-022-09260-7

Liu DS, Tan KC, Goh CK, et al., 2007. A multiobjective memetic algorithm based on particle swarm optimization. *IEEE Transactions on Systems, Man, and Cybernetics, Part B (Cybernetics)*, 37(1):42-50.
https://doi.org/10.1109/Tsmcb.2006.883270

Liu YY, Xi JL, Bai HF, et al., 2021. A general robot inverse kinematics solution method based on improved PSO algorithm. *IEEE Access*, 9:32341-32350.
https://doi.org/10.1109/Access.2021.3059714

Luo X, Zhang YJ, Zhang L, 2021. Study of error compensations and sensitivity analysis for 6-DOF serial robot. *Engineering Computations*, 38(4):1851-1868.
https://doi.org/10.1108/Ec-03-2020-0128

Navarro J, Segarra P, Sanchidrián JA, et al., 2019. Assessment of drilling deviations in underground operations. *Tunnelling and Underground Space Technology*, 83:254-261.
https://doi.org/10.1016/j.tust.2018.10.003

Raghavan M, Roth B, 1993. Inverse kinematics of the general 6R manipulator and related linkages. *Journal of Mechanical Design*, 115(3):502-508.
https://doi.org/10.1115/1.2919218

Sethu TA, Letsebe TP, Magwaza L, et al., 2017. Introduction of drill and blast utilizing pneumatic rock-drills in a Rwandan artisanal underground mine. *Journal of the Southern African Institute of Mining and Metallurgy*, 117(4):313-319.
https://doi.org/10.17159/2411-9717/2017/v117n4a1

Song CG, Yao LH, Hua CY, et al., 2021. Comprehensive water quality evaluation based on kernel extreme learning machine optimized with the sparrow search algorithm in Luoyang river basin, China. *Environmental Earth Sciences*, 80(16):521.
https://doi.org/10.1007/s12665-021-09879-x

Tsagaris A, Mansour G, 2019. Path planning optimization for mechatronic systems with the use of genetic algorithm and ant colony. *IOP Conference Series: Materials Science and Engineering*, 564(1):012051.
https://doi.org/10.1088/1757-899X/564/1/012051

Wang XQ, Cao JF, Liu X, et al., 2020. An enhanced step-size Gaussian damped least squares method based on machine learning for inverse kinematics of redundant robots. *IEEE Access*, 8:68057-68067.
https://doi.org/10.1109/Access.2020.2986421

Wang YJ, Fang C, Jiang QM, et al., 2015. The automatic drilling system of 6R-2P mining drill jumbos. *Advances in Mechanical Engineering*, 7(2):504861.
https://doi.org/10.1155/2015/504861

Wu D, Hou GW, Qiu WJ, et al., 2021. T-IK: an efficient multi-objective evolutionary algorithm for analytical inverse kinematics of redundant manipulator. *IEEE Robotics and Automation Letters*, 6(4):8474-8481.
https://doi.org/10.1109/Lra.2021.3108550

Yu DY, 2021. A new pose accuracy compensation method for parallel manipulators based on hybrid artificial neural network. *Neural Computing and Applications*, 33(3):909-923.
https://doi.org/10.1007/s00521-020-05288-6

Yuan PJ, Chen DD, Wang TM, et al., 2018. A compensation method based on extreme learning machine to enhance absolute position accuracy for aviation drilling robot. *Advances in Mechanical Engineering*, 10(3):168781401876341
https://doi.org/10.1177/1687814018763411

Zeng YF, Tian W, Li DW, et al., 2017. An error-similarity-based robot positional accuracy improvement method for a robotic drilling and riveting system. *The International Journal of Advanced Manufacturing Technology*, 88(9-12):2745-2755.
https://doi.org/10.1007/s00170-016-8975-8

Zhang DM, Hannaford B, 2019. IKBT: solving symbolic inverse kinematics with behavior tree. *Journal of Artificial Intelligence Research*, 65:457-486.
https://doi.org/10.1613/jair.1.11592

Zhang L, Xiao NF, 2019. A novel artificial bee colony algorithm for inverse kinematics calculation of 7-DOF serial manipulators. *Soft Computing*, 23(10):3269-3277.
https://doi.org/10.1007/s00500-017-2975-y

Zhang T, Du L, Dai XL, 2014. Test of robot distance error and compensation of kinematic full parameters. *Advances in Mechanical Engineering*, 6:810684.
https://doi.org/10.1155/2014/810684